Supplement to Small et al.

S1. GPR survey

Following an initial preliminary line a survey grid was marked out on the northern side of Patch Rock. The survey lines were aligned perpendicular to the inferred subglacial ridge. The lines (Line 1 – Line 5) were spaced at 10 m intervals with an additional two lines (Line 6 – Line 7) spaced at 20 m intervals (Fig. S1). The survey indicated that bedrock was located at accessible depths immediately beneath areas of blue ice.

Data processing followed steps outlined in the literature (cf. Winter et al., 2016) with some heuristic modification of parameters. All data processing was undertaken in Sandemeir ReflexW software v9.5 (Sandmeier Scientific Software, 2019). We applied a time-zero correction, de-wow, energy-decay gain, background removal, and a bandpass filter. Finally, we rubber-banded the data using the marker interpolation function. For time-depth conversion we used a nominal value of 0.168 m ns -1 for glacial ice (Winter et al., 2016). Given the shallow depths and glaciological setting in a zone of blue ice it is reasonable to assume no variation with depth.

Fig. S1. Google Earth imagery of Plummer Nunatak (© Google 2025) showing the layout of the survey lines used to characterise the subglacial morphology. The locations of flags used as fiducial markers is also shown. The snowfield surrounding Patch Rock/Plummer Nunatak can be seen.

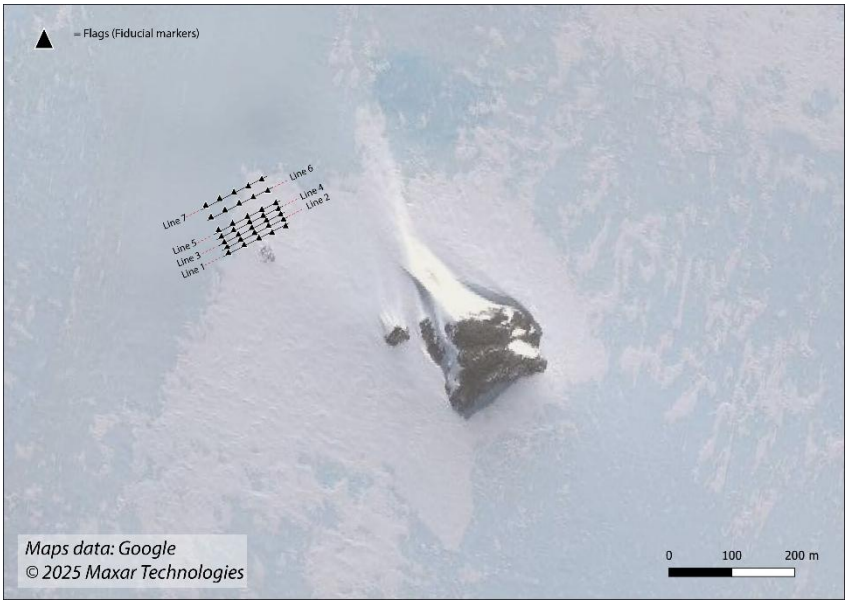

Table S1. Parameters used in GPR survey and summary of processing steps applied.

Parameter	Value
Antenna frequency	100 MHz
Antenna separation	1 m
Time window	1800 ns
Sampling interval	0.8 ns
Stepsize	1 m (so = trace no.)
Stacking	64
Processing steps	Time zero correction
	De-wow
	Energy decay gain
	Background removal
	Bandpass filter

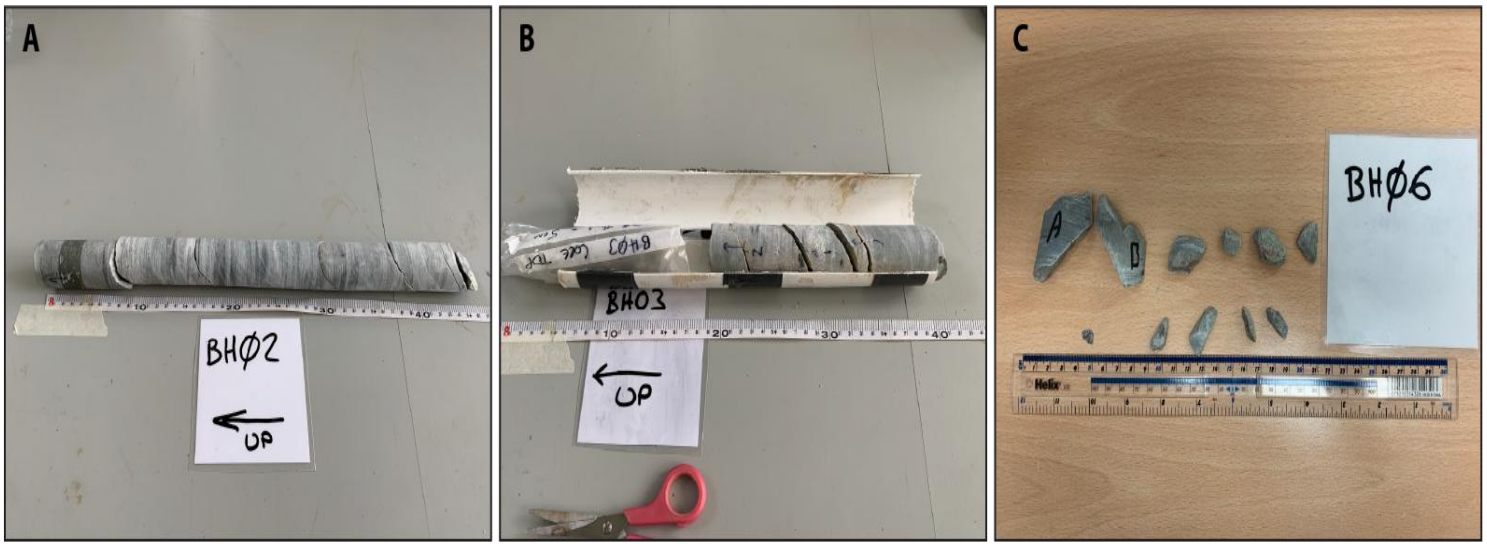

Fig. S2. Photographs of bedrock cores collected during austral summer of 2022-2023. Core top of BH03 (in bag) consisted of loose fragments of bedrock recovered from immediately above the core.

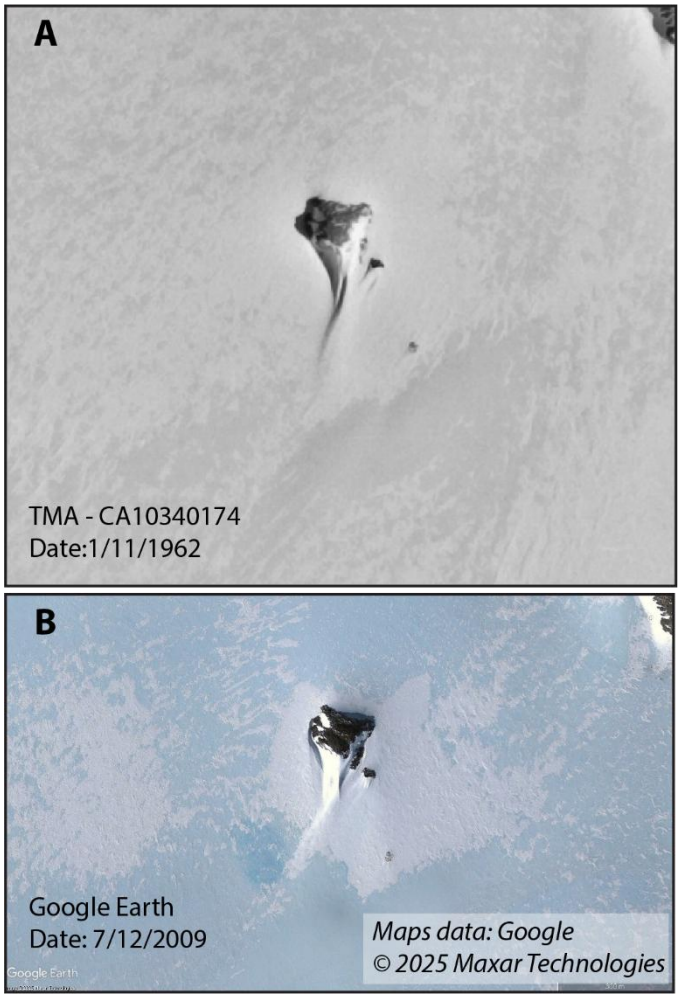

Fig. S3. Panel A shows TMA air photograph of Plummer Nunatak taken in 1962. Patch Rock can be seen below and to the right of the main outcrop. Panel B shows equivalent field of view in 2009 from Google Earth ((© Google 2025) showing no clear change in visible extent of outcrop. The extent observed in 2022-23 was also the same.

S2. Luminescence measurements

The core from BH01 was recovered in the dark to facilitate analysis using rock surface luminescence. The sample was prepared at the University of Liverpool luminescence laboratory under subdued-lighting conditions to prevent sunlight contamination of the luminescence signal. Due to the irregular core-top morphology, a single luminescence-sample core (7 mm diameter) was drilled into the top surface using an Axminster bench-top, pillar drill equipped with a water-cooled, diamond-tipped drill bit. The core was sliced at a thickness of ~0.7 mm using a Buehler IsoMet low-speed saw equipped with a water-cooled, 0.3 mm diameter diamond-tipped wafer blade. Slices were mounted in stainless steel cups for luminescence measurements.

Luminescence measurements were performed on a Risø TL/OSL reader (TL-DA-15) with a $^{90}Sr/^{90}Y$ beta irradiation source. Blue signals of quartz were detected in UV wavelengths using a photomultiplier tube fitted with a U340 filter (5 mm thickness). A preheat of 220 °C was used prior to a blue stimulation at 125 °C for 60 s. Luminescence depth profiles were determined by measuring the natural signal (L_n) normalised using the signal measured in response to a 49 Gy test-dose (T_n), termed the L_n/T_n signal. The luminescence signal was determined by subtracting the background signal (final 20 s, 40 channels) from the initial signal (0 – 3.5 s, 7 channels). The Ln/Tn values were interpolated on to a dose-response curve constructed from progressively larger laboratory doses to determine a De value for each rock slice. Sensitivity tests to assess whether the initial integration limits impact upon calculated D_e values showed that changing the initial integration limits from 0.5 to 3.5 s generally had little impact upon the D_e values calculated although there was a small difference for the surface slice where the shorter initial signal integrations generated slightly large D_e values (Fig. S4). Rock slices from BH01 were used for dose-recovery experiments after a 7 h bleach in a Hoenle UVACUBE 400. A 58 Gy given dose was administered to five discs after artificial bleaching and was successfully recovered to within 10% (dose-recovery ratio of 1.01 ± 0.03) demonstrating suitable analysis protocol.

Given that the luminescence signal emitted from the rock slices may originate from both quartz and K-feldspar as they can't be physically separated, anomalous fading experiments were performed using a given dose of 80 Gy and a maximum delay time of 10 h. It is thought that the fast component of a quartz luminescence signal does not fade and so if a large fading rate is measured, it is likely an indication that the signal used for dating is not suitable. The fading rate measured for sample BH01 was 9.2 ± 2.3 % per decade from three aliquots.

S2.1 Environmental dose-rates

To calculate the environmental dose-rate throughout burial for each sample, U, Th and K concentrations were measured for each rock core (grainsize of 90-110 µm) using high-resolution gamma spectrometry (Table S2). Cosmic dose-rates were calculated after Prescott and Hutton (1994) based on a depth below ice surface of 10 ± 1 m. The water contents of the rocks were assumed to be negligible (after Jenkins et al. 2018). An a-value of 0.10 ± 0.02 (Olley et al. 1998) was used to calculate the alpha dose-rates for quartz. Finally, the variation of the dose-rate with depth into each cobble surface was determined using the model proposed by Freiesleben et al. (2015) and Jenkins et al. (2018) were used to calculate depth-specific ages (Riedesel and Autzen, 2020, 2024). The matrix overlying the bedrock core was inert ice, which provided a negligible dose-rate; thus, only the dose-rate originating from the bedrock core itself was used for age calculation.

S2.2 Rock composition

After luminescence measurements were performed, each rock slice was analysed to investigate potential changes in rock composition with depth. Down-core red-green-blue (RGB) values were determined for each sample to investigate whether there was any colour variation within the sample, and externally between samples; thus, providing a semi-quantitative tool to detect variability in rock opacity (Meyer et al. 2018). Raster images of RGB were obtained for each rock slice using an EPSON Expression 11000XL flatbed scanner at 1200 dpi resolution. Mean and standard deviations of the RGB values (Fig. S5) for each rock slice were calculated using the *raster* package in R (version 2.9-23; Hijmans, 2015). The average down-core grainsize of each sample was measured using *ImageJ*. For each rock slice of an example core per sample, ten randomly selected grains were measured, and the mean and standard deviation grainsize were calculated per core. Scanning electron microscope energy dispersive x-ray spectroscopy (SEM-EDS) images mapping the distribution of K across rock slices of sample BH01 showed that the rock slices contained large proportions of K-rich minerals (Fig. S6).

	Value	Error
U (ppm)	4.81	1.35
TH (ppm)	26.98	0.24
K (%)	4.74	0.24
Ext. alpha dose rate (Gy/ka)	0.79	0.13
Ext. beta dose rate (Gy/ka)	5.11	0.20
Ext. gamma dose rate (Gy/ka)	1.78	0.09
Cosmic dose-rate (Gy/ka)	0.20	0.02
Total does rate (Gy/ka)	7.877	0.259

Table S2. U, Th and K concentrations used to calculate environmental dose rate contributions

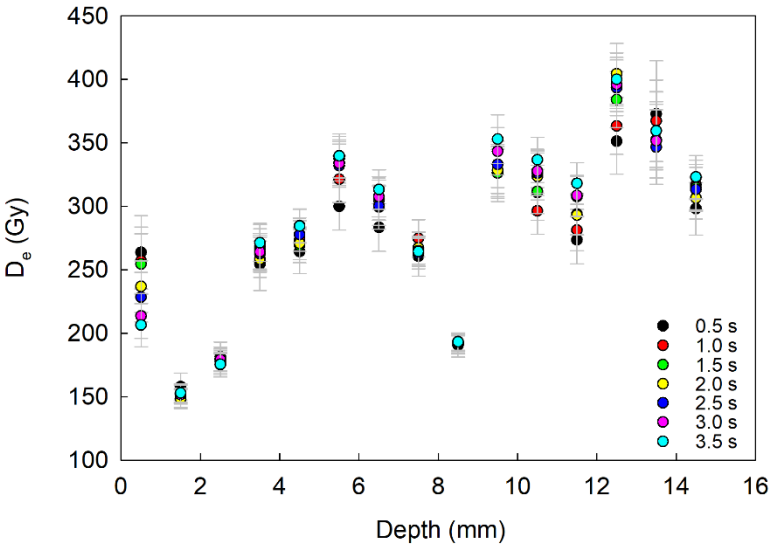

Fig. S4. Effect of choice of integration limits on calculated De values at all depths in BH01.

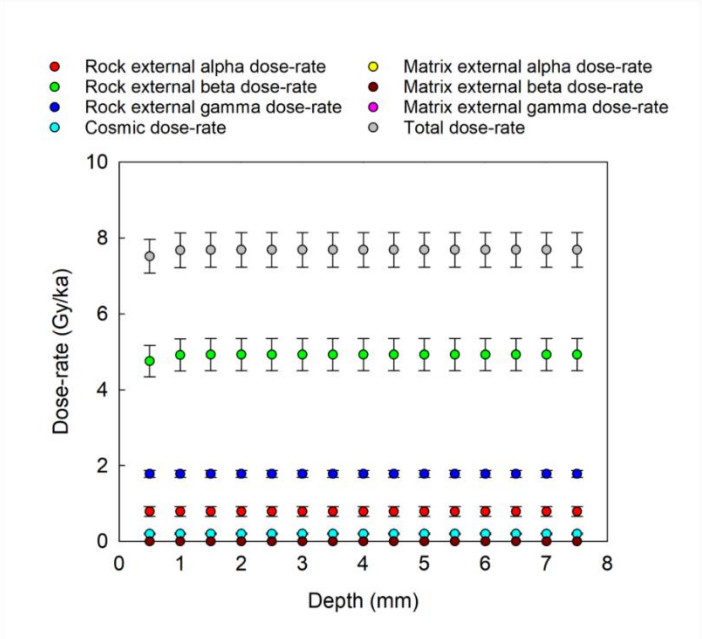

Fig. S5. Variation in dose-rate with depth determined (Freiesleben et al. 2015); Jenkins et al. 2018). The matrix overlying the bedrock core was inert ice, which provided a negligible dose-rate.

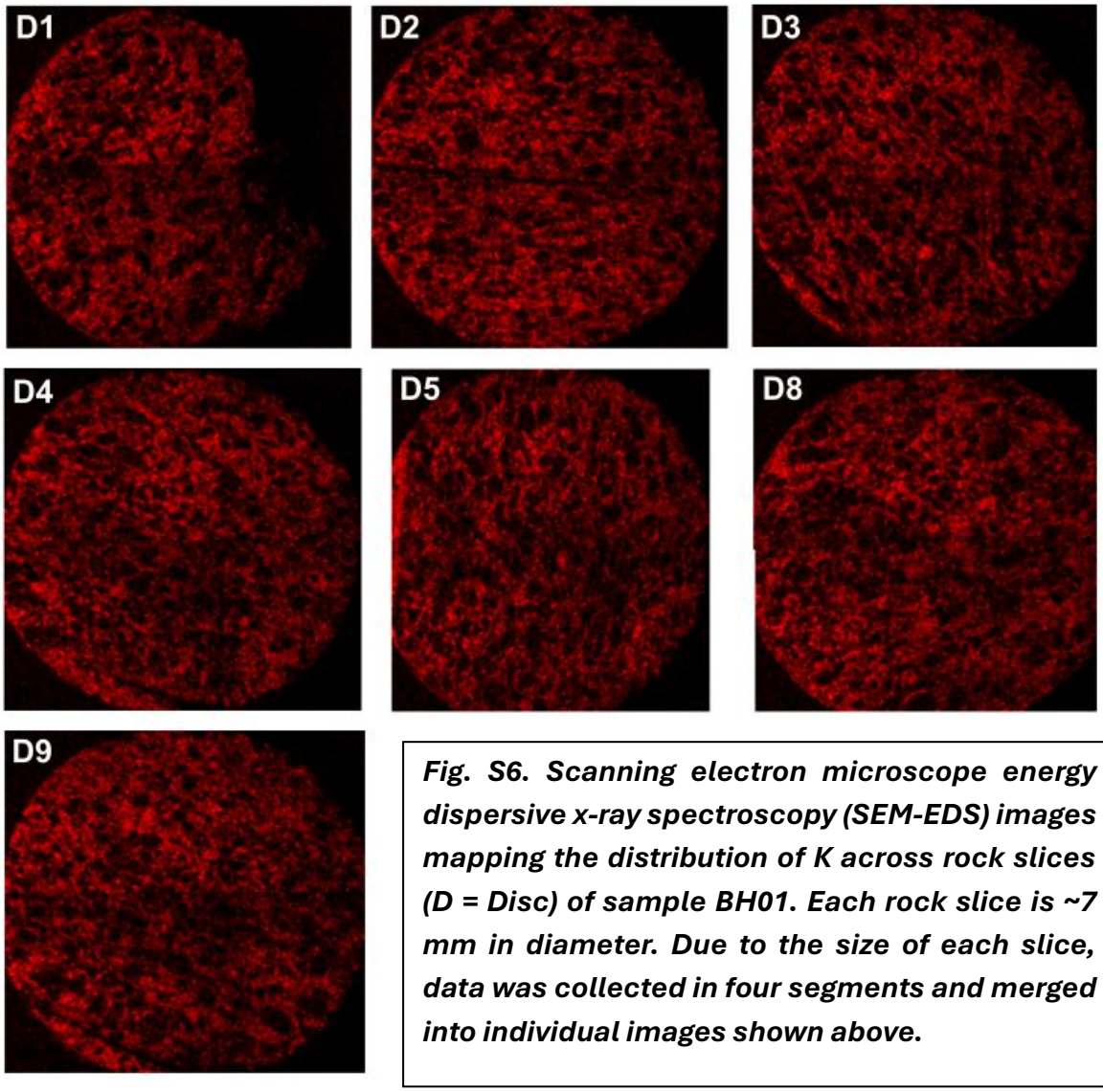

Fig. S6. Scanning electron microscope energy dispersive x-ray spectroscopy (SEM-EDS) images mapping the distribution of K across rock slices (D = Disc) of sample BH01. Each rock slice is ~7 mm in diameter. Due to the size of each slice, data was collected in four segments and merged into individual images shown above.

Fig. S7. Profiles showing measured RGB values which are interpreted as a proxy for rock opacity.

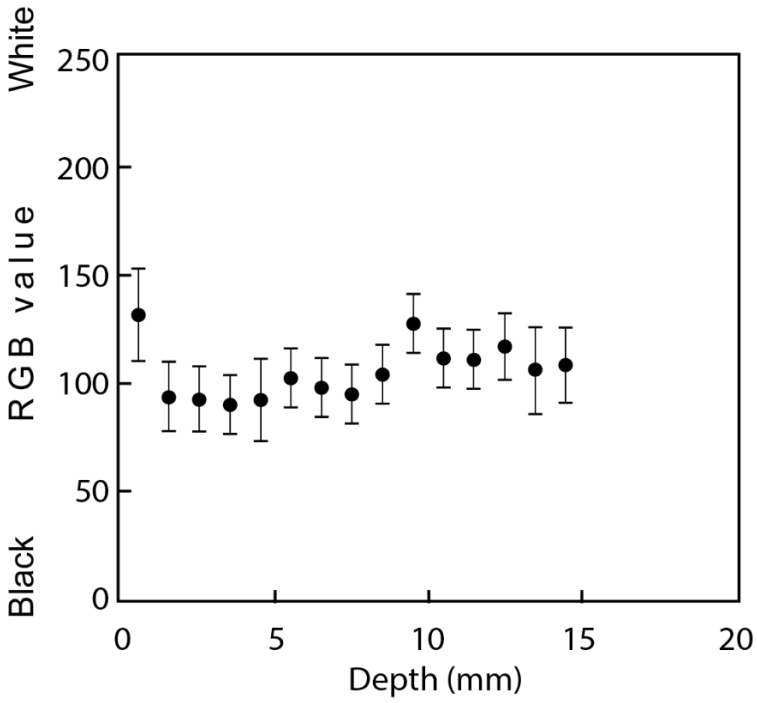

Disc number	Depth into rock surface (mm)	Normalised luminescence (a.u.)	Error	De value (Gy)	Error (Gy)	Environmental dose-rate (Gy/ka)	Error (Gy/ka)	Age (ka)	Error (ka)
1	0.5	0.68	0.05	206.32	17.01	7.52	0.44	27.4	2.8
2	1.5	0.48	0.02	152.82	7.27	7.68	0.46	19.9	1.5
3	2.5	0.56	0.03	175.48	8.36	7.69	0.46	22.8	1.7
4	3.5	0.78	0.04	271.27	14.60	7.69	0.46	35.3	2.8
5	4.5	0.79	0.04	284.43	13.21	7.69	0.46	37.0	2.8
6	5.5	0.85	0.04	339.77	17.18	7.69	0.46	44.2	3.4
7	6.5	0.83	0.04	313.29	15.58	7.69	0.46	40.7	3.2
8	7.5	0.76	0.04	264.40	11.38	7.69	0.46	34.4	2.5
9	8.5	0.61	0.03	193.13	6.74	7.69	0.46	25.1	1.7
10	9.5	0.91	0.05	352.97	19.29	7.69	0.46	45.9	3.7
11	10.5	0.86	0.04	336.64	17.80	7.69	0.46	43.8	3.5
12	11.5	0.85	0.04	318.03	16.36	7.69	0.46	41.4	3.3
13	12.5	1.00	0.05	400.06	20.89	7.69	0.46	52.0	4.1
14	13.5	0.89	0.05	359.58	30.84	7.69	0.46	46.8	4.9
15	14.5	0.81	0.04	323.15	17.00	7.69	0.46	42.0	3.3

Table S3. Raw and normalised Ln/Tn ratios from bedrock core BH01.

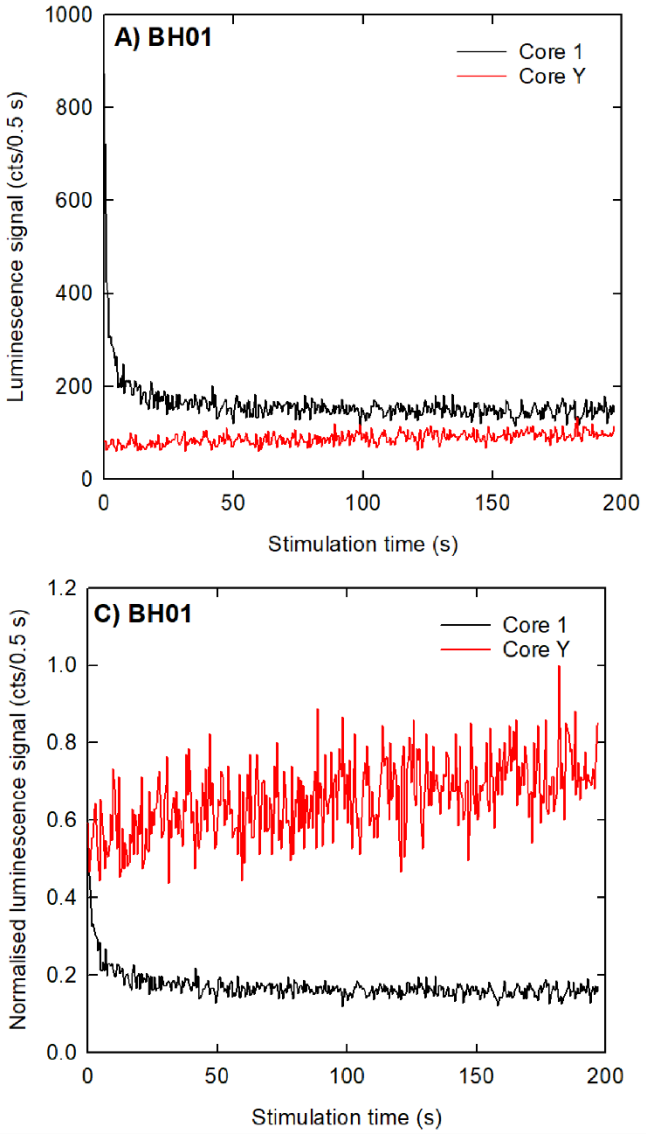

Fig. S8 Luminescence signals emitted in response to a fixed 49 Gy test-dose for example slices from sample BH01 stimulated with blue wavelengths, measured in UV wavelengths, expected to be dominated by quartz.

S3. *In situ* ^{14}C sample processing

S3.1 Quartz purification and carbon extraction

Samples were crushed and sieved to 125 – 500 µm at Durham University before being sent to the Scottish Universities Environmental Research Centre (SUERC) Cosmogenic Nuclide Facility. Quartz was purified using successive leaches in 1% HF/HNO_3. Sample purity was assessed using ICP-OES. Some samples exhibited significant quantities in the 75-125 µm fraction, presumably due to progressive disaggregation and fracturing of polycrystalline grains. This is likely due to the mineralogy of the bedrock which exhibited small detrital quartz grains and extensive interstitial overgrowths (Fig. S9). Samples underwent additional pre-cleaning prior to carbon extraction including an etch in concentrated HNO_3 at 140°C and subject to *in-vacuo* cleaning at 600 °C to remove meteoric ^{14}C. Measurement of CRONUS-A using the same pre-treatment protocols as our samples gives a value of $5.85 \times 10^5 \pm 0.40 \times 10^5$ atoms g^{-1}.

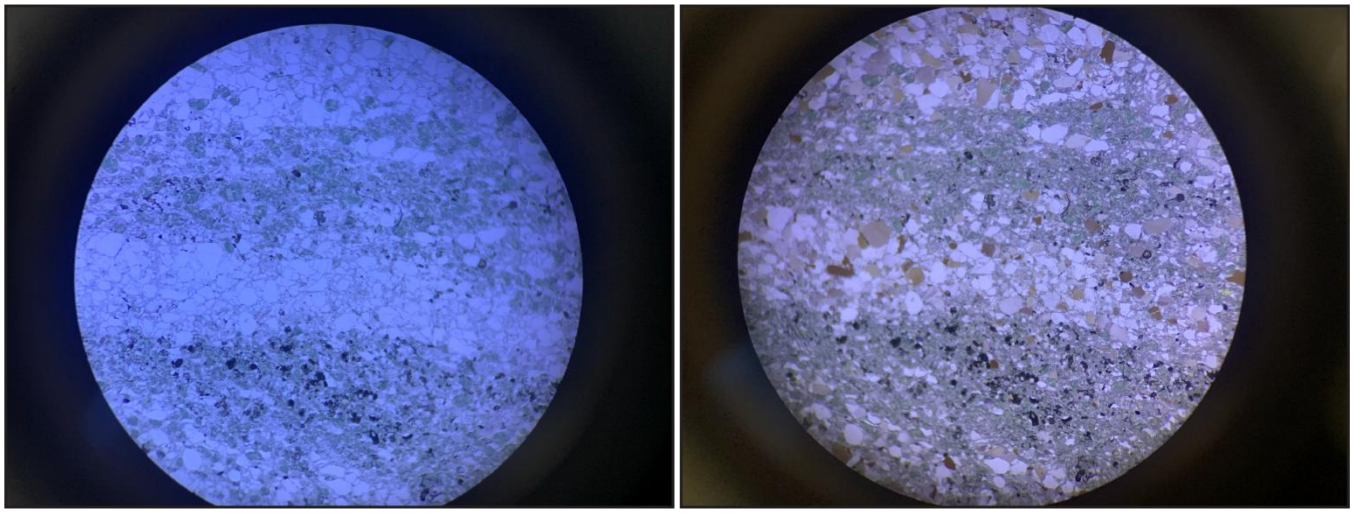

Fig. S9. Thin section photographs of Crashsite quartz arenite (or quartzite) in plane-polarized light (left) and cross-polarized light (right). The generally small size of the detrital quartz grains can be seen.

Extraction of *in situ* consists of (i) Sealing pre-cleaned quartz aliquots in fused silica tubes, (ii) transformation of quartz to cristobalite by heating at 1650°C for 2 hours under a continuous flow of nitrogen gas, releasing ^{14}C as CO_2; (iii) *in-vacuo* cracking of the silica tubes to release collected gas. This is subsequently cleaned and the mass of CO_2 quantified using a capacitance manometer (cf. Fülöp et al., 2019). The cleaned CO_2 gas is converted to graphite using the in-house laser-heated microfurnace at ANSTO (Yang et al., 2015). The graphitized targets are then ready for analysis using accelerator mass spectrometry (AMS) at the ANSTO AMS facility.

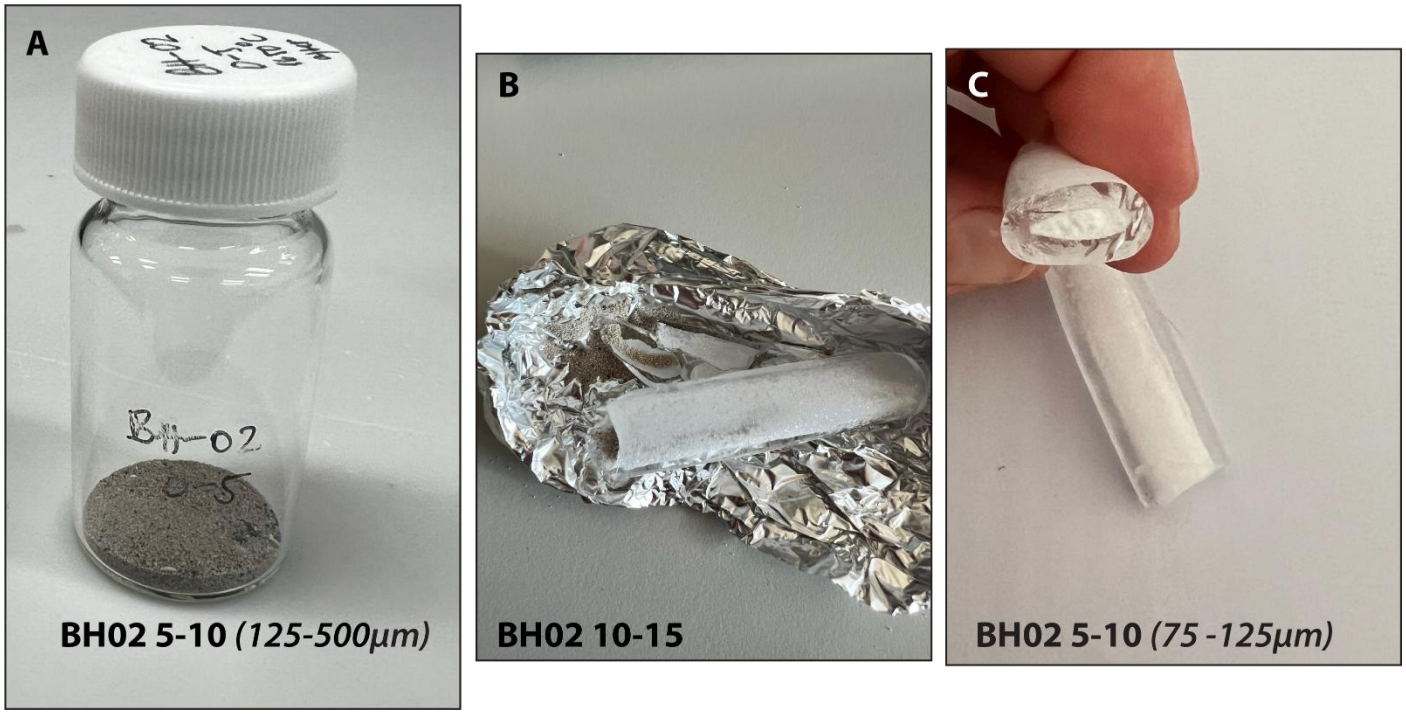

Fig. S10. Examples of samples following carbon extraction A) and B) show discolorations that are considered indicative of contamination. A) Initial extraction of BH02 0-5 cm (125-500 µm). B) Sample BH02 10-15 cm, no additional material was prepared thus this sample was not analysed. C) Sample BH02 5-10 cm (75-125 µm) shows no discolouration and is representative of other samples following extraction.

Analysis of CRONUS-N reference material (Jull et al., 2015) at ANSTO yields blank corrected concentrations of 1.77 x 10^4 – 1.26 x 10^4 atoms g^{-1} (Table S5). This is comparable to previously reported values for this reference material (i.e., Lupker et al., 2019). The CRONUS-N material is a beach sand that contains infrequent impurities and has a low in situ ^{14}C concentration. As such it is inherently similar to the samples presented here. The fact that the measured concentrations of CRONUS-N are consistent with the reported values gives us additional confidence that the reported concentrations presented here represent in situ ^{14}C that is present within our samples.

Sample details	Grain size	Oz-Code	pmC	Δ [pmC]	C [µg]	Mass (g)	N_{14} [at]	Δ N_{14} [at]	Blk-corr. N_{14} [at]	Blk-corr. Δ N_{14} [at]	N_{14} [at/g]	Δ N_{14} [at/g]	ugC/g
CRN-46	125-500	5817	11.06	0.43	7.67	2.0281	51300	1616	35814	9584	17659	4726	3.78
CRN-47	125-250	5817	10.08	0.62	7.19	2.0878	45082	1756	29597	9609	14176	4602	3.44
CRN-48	125-250	5817	10.76	0.78	6.77	2.0272	41118	1560	25632	9575	12644	4723	3.34

Table S5. Nuclide concentrations of three measurements of aliquots of CRONUS-N reference material using sample preparation protocols relevant to this study.

S4. Supplementary references

Aitken, M.J., 1998. *Introduction to optical dating: the dating of Quaternary sediments by the use of photon-stimulated luminescence*. Clarendon Press.

Freiesleben, T., Sohbati, R., Murray, A., Jain, M., Al Khasawneh, S., Hvidt, S. and Jakobsen, B., 2015. Mathematical model quantifies multiple daylight exposure and burial events for rock surfaces using luminescence dating. *Radiation Measurements*, *81*, pp.16-22.

Fülöp, R.H., Fink, D., Yang, B., Codilean, A.T., Smith, A., Wacker, L., Levchenko, V. and Dunai, T.J., 2019. The ANSTO–University of Wollongong in-situ 14C extraction laboratory. *Nuclear Instruments and Methods in Physics Research Section B: Beam Interactions with Materials and Atoms*, *438*, pp.207-213.

Jenkins, G.T.H., Duller, G.A.T., Roberts, H.M., Chiverrell, R.C. and Glasser, N.F., 2018. A new approach for luminescence dating glaciofluvial deposits-High precision optical dating of cobbles. *Quaternary Science Reviews*, *192*, pp.263-273.

Jull, A.T., Scott, E.M. and Bierman, P., 2015. The CRONUS-Earth inter-comparison for cosmogenic isotope analysis. *Quaternary Geochronology*, *26*, pp.3-10.

Lupker, M., Hippe, K., Wacker, L., Steinemann, O., Tikhomirov, D., Maden, C., Haghipour, N. and Synal, H.A., 2019. In-situ cosmogenic 14C analysis at ETH Zürich: Characterization and performance of a new extraction system. *Nuclear Instruments and Methods in Physics Research Section B: Beam Interactions with Materials and Atoms*, *457*, pp.30-36.

Hijmans, R.J., Van Etten, J., Cheng, J., Mattiuzzi, M., Sumner, M., Greenberg, J.A., Lamigueiro, O.P., Bevan, A., Racine, E.B., Shortridge, A. and Hijmans, M.R.J., 2015. Package 'raster'. *R package*, *734*, p.473.

Meyer, M.C., Gliganic, L.A., Jain, M., Sohbati, R. and Schmidmair, D., 2018. Lithological controls on light penetration into rock surfaces–Implications for OSL and IRSL surface exposure dating. *Radiation Measurements*, *120*, pp.298-304.

Olley, J., Caitcheon, G. and Murray, A., 1998. The distribution of apparent dose as determined by optically stimulated luminescence in small aliquots of fluvial quartz: implications for dating young sediments. *Quaternary Science Reviews*, *17*(11), pp.1033-1040.

Prescott, J.R. and Hutton, J.T., 1994. Cosmic ray contributions to dose rates for luminescence and ESR dating: large depths and long-term time variations. *Radiation measurements*, *23*(2-3), pp.497-500.

Riedesel, S., Autzen, M., 2020. Beta and gamma dose rate attenuation in rocks and sediment. *Radiation Measurements 133*, 106295.

Riedesel, S., Autzen, M., 2024. calc_CobbleDoseRate(): Calculate dose rate of slices in a spherical cobble. Function version 0.1.0. In: Kreutzer, S., Burow, C., Dietze, M., Fuchs, M.C., Schmidt, C., Fischer, M., Friedrich, J., Mercier, N., Philippe, A., Riedesel, S., Autzen, M., Mittelstrass, D., Gray, H.J., Galharret, J., Colombo, M., 2024. Luminescence: Comprehensive Luminescence Dating Data Analysis. R package version 0.9.25. https://r-lum.github.io/Luminescence/

Sandmeier Scientific Software (2019), ReflexW, version 9.5 [Available to download from **http://www.sandmeier-geo.de/download.html**.]

Winter, K., Woodward, J., Dunning, S.A., Turney, C.S., Fogwill, C.J., Hein, A.S., Golledge, N.R., Bingham, R.G., Marrero, S.M., Sugden, D.E. and Ross, N., 2016. Assessing the continuity of the blue ice climate record at Patriot Hills, Horseshoe Valley, West Antarctica. *Geophysical Research Letters*, *43*(5), pp.2019-2026.

Yang, B., Smith, A.M. and Long, S., 2015. Second generation laser-heated microfurnace for the preparation of microgram-sized graphite samples. *Nuclear Instruments and Methods in Physics Research Section B: Beam Interactions with Materials and Atoms*, *361*, pp.363-371.